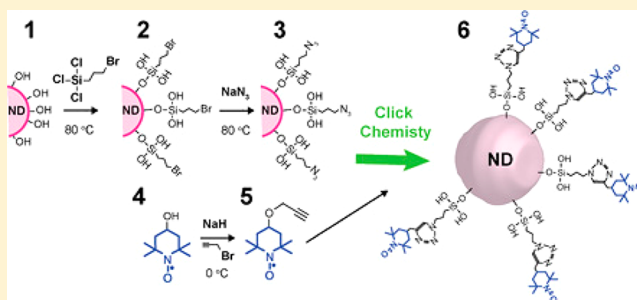


# Grafting Nitroxide Radicals on Nanodiamond Surface Using Click Chemistry

Ekaterina E. Romanova,<sup>†</sup> Rana Akiel,<sup>†</sup> Franklin H. Cho,<sup>‡</sup> and Susumu Takahashi<sup>\*,†,‡</sup>

<sup>†</sup>Department of Chemistry and <sup>‡</sup>Department of Physics, University of Southern California, Los Angeles, California 90089, United States

**ABSTRACT:** We demonstrate grafting of nitroxide radicals on the surface of nanodiamonds (NDs). The surface of NDs is functionalized by azide groups. Nitroxide radicals are covalently bonded using Cu(I)-catalyzed azide/alkyne-click chemistry approach. The reaction is confirmed by infrared spectroscopy. The grafting of nitroxides is also verified by studying the rotational correlational time using electron paramagnetic resonance (EPR) spectroscopy. EPR study estimates that a few hundreds (tens) of nitroxide radicals are grafted on the surface of NDs with 100 nm (25 nm) of the average diameter.



## INTRODUCTION

Nanodiamonds (NDs) are fluorescent nanometer-sized particles with excellent mechanical and chemical stability. NDs have recently been investigated extensively because of unique optical and magnetic properties of nitrogen-vacancy (NV) impurity color centers in NDs. NV centers are attractive for testing fundamental quantum science<sup>1–4</sup> and for future applications of magnetic sensing devices.<sup>5–8</sup> In addition, biocompatibility and photostability of fluorescent NDs make them suitable for optical and magnetic imaging of biological systems and for drug delivery by functionalizing their surface to attach various types of molecules.<sup>9–21</sup> Several approaches to control surface functionalization for NDs have been investigated. Examples include treatment of NDs with oxidizing reagents,<sup>22</sup> silanization of the hydroxylated NDs,<sup>23</sup> fluorination,<sup>24</sup> or hydrogenation<sup>25,26</sup> of ND's surface using fluorine or hydrogen gases and elevated temperatures, followed by subsequent amination or thiolation. Most of these approaches require harsh reaction conditions, such as high temperatures, use of toxic gases, and sophisticated setups. One of the common ways to achieve homogeneous surface functionalization is employment of silanization technique.<sup>27</sup> Surface homogenization is often required for a high performance and reproducibility of subsequent reactions. The silanization technique has been widely applied to functionalize metal<sup>28,29</sup> and semiconductor<sup>30–32</sup> nanoparticles.

Cu(I)-catalyzed azide–alkyne cycloaddition (CuAAC) reaction known as click chemistry<sup>33</sup> has been utilized in a variety of approaches to graft various molecules on nanoparticle's surface.<sup>34</sup> The click chemistry proceeds at room temperature under mild reaction conditions and combines azide- and alkyne-containing reactants to give stable 1,4-disubstituted-1,2,3-triazole linker between nanoparticle surface and grafted molecule. The main advantage of the CuAAC application on surfaces is high efficiency, the avoidance of high temperatures,

as well as tolerance toward many functional groups. Therefore the click chemistry concept currently is one of the most versatile methods for grafting molecules on nanoparticle surface and has been successfully applied to various nanoparticles, such as Au,<sup>35</sup> CdSe,<sup>36</sup> Fe<sub>2</sub>O<sub>3</sub>,<sup>37</sup> SiO<sub>2</sub>,<sup>38</sup> and NDs.<sup>39,40</sup>

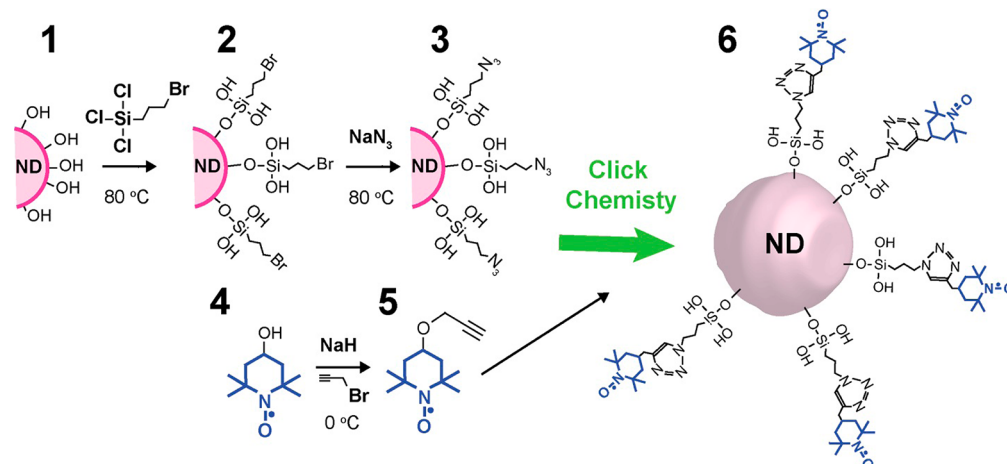
In this article, we demonstrate grafting of nitroxide radicals onto the surface of high-temperature high-pressure (HTHP) NDs with an average particle diameter of 100 and 25 nm. A covalent attachment of nitroxide radicals provides a way to stably position paramagnetic molecules on the ND surface for future applications of NV-based magnetic sensing and single-molecule magnetic resonance spectroscopy. For the grafting, we employ surface silanization and bromine–azide conversion to functionalize the ND surface with azide groups. A click-chemistry approach is employed to covalently attach alkyne-containing nitroxide radicals on the azide-functional ND surface. To the best of our knowledge, the combination of the surface silanization and click-chemistry for grafting organic molecules on ND surface has not been explored so far. The reaction process is confirmed using Fourier-transformed infrared (FTIR) and electron paramagnetic resonance (EPR) spectroscopies. We find that efficiency of click-chemistry approach is ~95% based on FTIR analysis. In addition, using EPR spectroscopy, we show that the rotational correlation time of nitroxides grafted on NDs is slower than that of free nitroxide radicals. The decrease in the correlation time strongly supports successful grafting of nitroxide radicals on the ND surface. The estimated number of nitroxides attached on a single 100 nm (25 nm) ND is ~300 (20).

**Special Issue:** Curt Wittig Festschrift

**Received:** March 31, 2013

**Revised:** June 1, 2013

Scheme 1. Cu(I)-Catalyzed Azide/Alkyne-Click Chemistry Approach for Grafting Nitroxide Radicals on the ND Surface (1–6)



## EXPERIMENTAL SECTION

**Materials and Chemicals.** We employed two kinds of HTHP ND powders; one has 100 nm average diameter (Engis, Wheeling, IL) and the other has 25 nm average diameter (Van Moppes, Geneva, Switzerland). For the synthesis of the nitroxide-grafted ND, the following chemicals were used: 3-bromopropyltrichlorosilane (#437808), 4-hydroxy-TEMPO (#176141), propargyl bromide (#P51001), borane tetrahydrofuran complex solution ( $\text{BH}_3\text{-THF}$ , #176192), sodium azide ( $\text{NaN}_3$ , #438456), sodium hydride ( $\text{NaH}$ , #223441), copper(I) iodide ( $\text{Cu(I)}$ , #205540), triethanolamine ( $\text{TEA}$ , #90279) and hydrochloric acid ( $\text{HCl}$ , #H1758) purchased from Sigma-Aldrich (Milwaukee, WI), dimethylformamide ( $\text{DMF}$ , #DX1729), ethyl acetoacetate ( $\text{ETOAC}$ , #8.09622), sulfuric acid ( $\text{H}_2\text{SO}_4$ , #1.00748), nitric acid ( $\text{HNO}_3$ , #NX0412), hexane (#HX0290), anhydrous acetonitrile ( $\text{CH}_3\text{CN}$ , #AX0152), and toluene (#TX0734) purchased from EMD Millipore (Billerica, MA). Milli-Q water (18 M $\Omega$ ) was used.

**Grafting of Nitroxide Radicals on ND Surface.** We employed Cu(I)-catalyzed azide/alkyne-click chemistry approach to graft nitroxide radicals on ND surfaces. Our synthesis procedure is shown in Scheme 1. To obtain the starting ND, ND surface was hydroxylated by performing a strong acid treatment, followed by a borane reduction. The acid treatment consists of refluxing NDs in a 9:1 mixture of concentrated  $\text{H}_2\text{SO}_4$  and  $\text{HNO}_3$  at 75 °C for 72 h, followed by 0.1 M  $\text{NaOH}$  solution at 90 °C for 2 h, then by 0.1 M  $\text{HCl}$  solution at 90 °C for 2 h. After the acid treatment, the obtained NDs were repeatedly rinsed with deionized (DI) water, separated by centrifugation (10 000–15 000 rpm for 15 min using Sorvall RC-5C Plus) and dried under vacuum. The acid cleaning removes graphitic and other organic impurities. It also oxidizes the ND surface, increasing the number of carboxyl groups ( $-\text{COOH}$ ). Subsequently, 6 mL of 1.0 M  $\text{BH}_3\text{-THF}$  was added dropwise to a stirring suspension of 250 mg acid-treated NDs in 30 mL of dry THF. Then, the mixture was refluxed for 24 h and hydrolyzed with 2 M  $\text{HCl}$  after cooling to room temperature. Resulting NDs were washed with DI water (four times) and acetone (once) in consecutive washing/centrifugation cycles to remove the boronic acid produced during the reaction and dried in vacuum to yield 230 mg of hydroxylated ND powder (**1**). To functionalize **1** with an azide group required for click chemistry, a silanization technique<sup>38</sup> was used. 230 mg of **1** and 20 mL of anhydrous toluene were first added

in a flask under a nitrogen atmosphere. The flask was sonicated for 30 min, then heated to 80 °C. One mL of 3-bromopropyltrichlorosilane was added dropwise and the resulting solution was heated to 80 °C for 24 h. To separate the product of bromide-functional NDs from unreacted 3-bromopropyltrichlorosilane, the reaction mixture was redispersed in toluene and centrifuged. This cycle was repeated four times to obtain 200 mg of pure bromide-functional NDs (**2**). Then, 200 mg of **2** and saturated solution of  $\text{NaN}_3$  (100 mg in 40 mL of  $\text{DMF}$ ) were combined in a flask under a nitrogen atmosphere. The mixture was sonicated for 30 min, then stirred at 80 °C for 24 h. The reaction mixture was redispersed in DI water and centrifuged to remove excess of sodium azide. This cycle was repeated four times to yield 175 mg of azide-functional NDs (**3**). Parallel to the synthesis of the azide-functional NDs, the alkyne-contained nitroxide radicals (**5**) were prepared from 4-hydroxy-TEMPO radicals (**4**). To a stirring suspension of  $\text{NaH}$  (175 mg) in 30 mL of dry  $\text{DMF}$ , 1 g of **4** was added at 0 °C. The solution was stirred at room temperature for 30 min, then 0.7 mL of propargyl bromide was added dropwise at 0 °C, followed by stirring for 3 h at room temperature. The reaction mixture was purified by column chromatography (silica gel, 10%  $\text{ETOAC}$  in hexane) to yield ~800 mg of **5**. Finally, covalent attachment of **5** and **3** was achieved by click-reaction in the presence of Cu(I) catalyst to yield nitroxide-grafted NDs (**6**). 175 mg of **3** was dispersed in 30 mL of anhydrous acetonitrile and sonicated for 30 min. The click-reaction was performed by the addition of 70 mg of **5**, 70 mg of Cu(I), and 1 mL of  $\text{TEA}$  to the mixture. The reaction was stirred for 48 h at room temperature, followed by centrifugation, and the pellet was resuspended in acetonitrile. This procedure was repeated 10–15 times to remove nonreacted nitroxide radicals. The resulting solid was dried in vacuum to yield **6**.

**Characterization.** Infrared (IR) spectra of functionalized NDs were measured using Bruker Vertex 80 FTIR spectrometer. In the IR measurement, dried ND powder (0.5 to 1 mg) was mixed with  $\text{KBr}$  powder (100 mg) in an agate mortar. The mixture was pressed into a pellet using a 10 ton load. In our FTIR measurement, FTIR signals from a pure  $\text{KBr}$  pellet were subtracted as background signals. Nitroxide radicals on the ND surface and paramagnetic impurities in and on NDs were characterized using EPR spectroscopy. We employed X-band continuous-wave (cw) EPR spectrometer (EMX system,

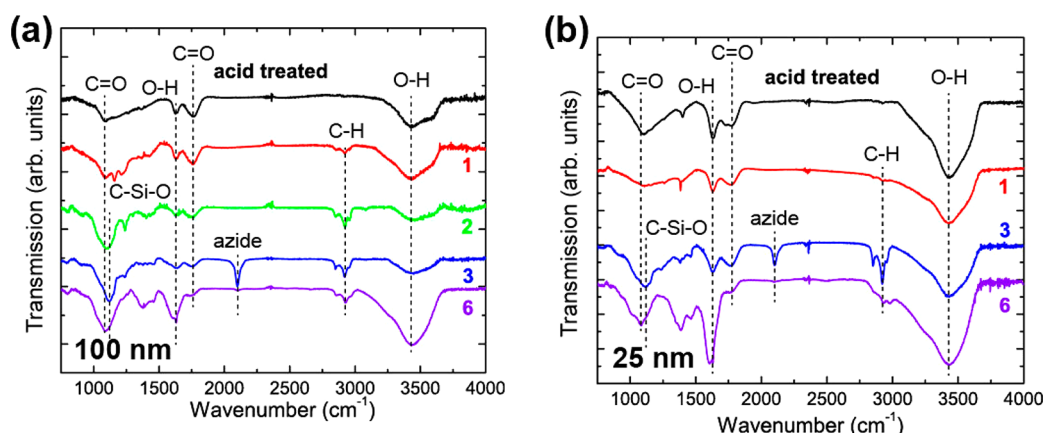


**Figure 1.** FTIR spectra of NDs. (a) FTIR signals of 100 nm NDs after acid treated and in 1, 2, 3, and 6 in Scheme 1. (b) FTIR signals of 25 nm NDs after acid treated and in 1, 3, and 6. FTIR signals from vibrational modes on the ND surface are indicated by dotted lines.

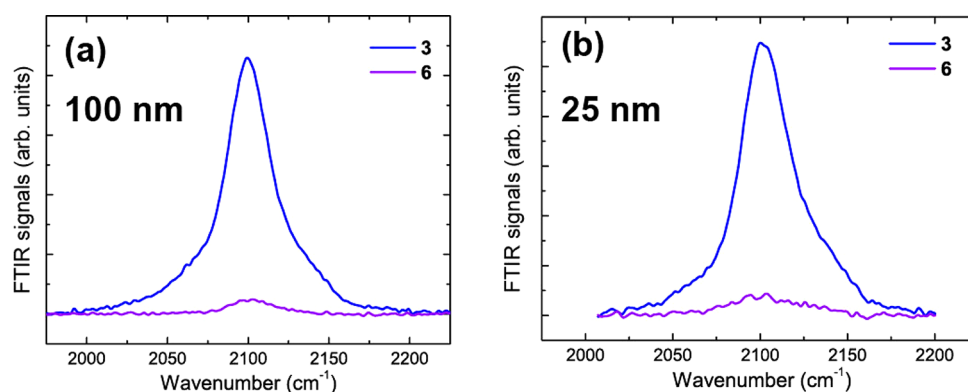


**Figure 2.** FTIR spectra of azide moieties at 2100 cm<sup>-1</sup>. (a) FTIR signals of 100 nm NDs in 3 and 6 in Scheme 1. (b) FTIR signals of 25 nm NDs in 3 and 6 in Scheme 1.

Bruker Biospin) with a high-sensitivity cavity (ER 4119HS, Bruker Biospin).

A home-built cw/pulsed 230/115 GHz EPR spectrometer was also employed to characterize nitroxide radicals and paramagnetic impurities. The high-frequency EPR system employs a high-power solid-state source consisting 8–10 GHz synthesizer, p-i-n switch, microwave amplifiers, and frequency multipliers. The output power of the source system is 100 mW (700 mW) at 230 GHz (115 GHz). 230/115 GHz excitation is propagated using quasi-optical bridge and a corrugated waveguide and couples to a sample located at the center of 12.1 T cryogenic-free superconducting magnet. EPR signals are isolated from the excitation using an induction mode operation.<sup>41</sup> For EPR detection, we employed a super-heterodyne detection system in which 230/115 GHz is down-converted into 3 GHz of intermediate frequency (IF), then down-converted again to in-phase and quadrature components of dc signals. Details of the system will be described elsewhere.

## RESULTS AND DISCUSSION

During the process of grafting nitroxide radicals on NDs, we measured FTIR spectrum of the NDs after each step of the reaction. Figure 1 shows the FTIR spectra of both 100 (a) and 25 nm (b) NDs after the acid treatment and after obtaining product of 1, 2, 3, and 6 in Scheme 1. The FTIR spectra of the acid-treated NDs show characteristic carbonyl (C=O) stretching vibration modes at ~1100 and ~1760 cm<sup>-1</sup> and

peaks of vibrational modes of hydroxyl groups (O–H) at ~1630 cm<sup>-1</sup> and in 3000–3600 cm<sup>-1</sup>.<sup>23</sup> The reaction with tetrahydrofuran complex typically reduces carbonyl groups to hydroxyl groups, that is, leading to decrease in the C=O IR signals and increase in the O–H and C–H IR signals. As shown in 1 in Figure 1, an increase in the C–H stretching vibrational signal (near 2992 cm<sup>-1</sup>) was visible, indicating increase of hydroxyl groups due to the reduction of carboxyl groups on ND surface. Changes of the O–H signals were not well-pronounced due to absorption signals of water molecules on ND surface. In addition, the remaining C=O signal in 1 suggested that the reduction step resulted in ND surface partially covered with hydroxyl groups. This is due to the fact that acid-treated NDs form strongly bounded agglomerates that are hard to separate by ultrasonication because of interparticle covalent bonding.<sup>23</sup> Therefore, the reducing agent will have limited access to ND surface, resulting in an inhomogeneous surface functionalization.

To obtain Product 2, we used the hydroxyl groups of 1 to covalently attach 3-bromopropyltrichlorosilane to ND surface. After the reaction, the binding of silane was confirmed by the characteristic FTIR signal of the C–Si–O bond at ~1119 cm<sup>-1</sup> shown in Figure 1a. Then, 2 were reacted with sodium azide to obtain azide-functional NDs (3). For both 100 and 25 nm NDs, the success of the reaction was confirmed by the appearance of azide signal at 2100 cm<sup>-1</sup> in the FTIR spectra of 3.<sup>37,38</sup> Finally, using click-reaction, alkyne-contained nitroxide radicals were covalently attached to 3 through the azide-

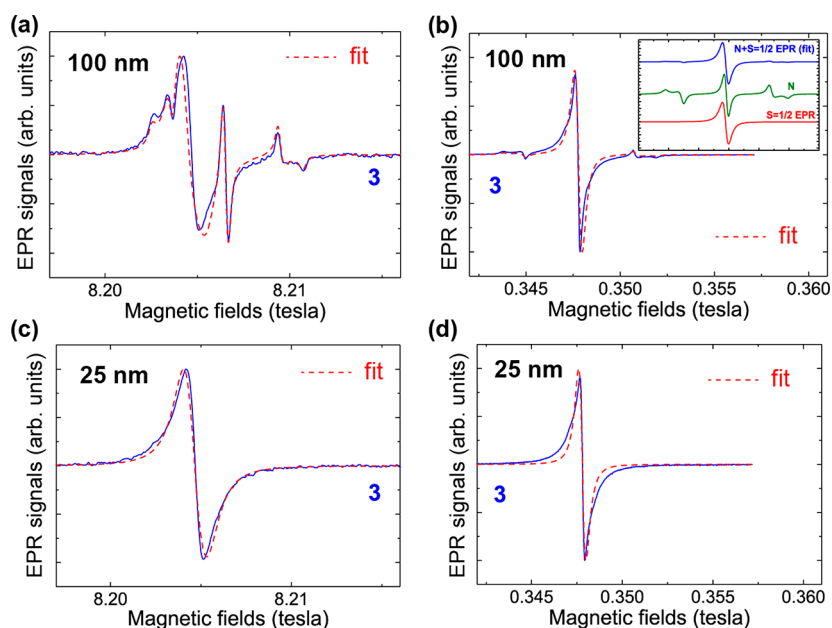


**Figure 3.** cw EPR spectra of the ND powder samples (Product 3 in Scheme 1). (a) 230 GHz EPR spectrum of 100 nm NDs. The spectrum includes N spin and the other  $S = 1/2$  impurities signals. A fit to the data using easyspin<sup>42</sup> is shown by the red dotted line. The fit gives  $g_{x,y} = 2.0029 \pm 0.0001$  and  $g_z = 2.0027 \pm 0.0001$  and  $0.8 \pm 0.1$  mT of Lorentzian peak-to-peak line width for the  $S = 1/2$  EPR signal, and the intensity ratio of N to the  $S = 1/2$  EPR is  $1:6 \pm 1$ . (b) X-band EPR spectrum of 100 nm NDs. A fit is shown by the red dotted line. For the fit, we used the  $g$  value for the  $S = 1/2$  spin obtained from the 230 GHz EPR measurement. The fit gives  $0.4 \pm 0.1$  mT of Lorentzian peak-to-peak line width and the intensity ratio (N to the  $S = 1/2$  EPR) is  $1:8 \pm 1$ . The inset shows the fitted EPR spectrum consisting of N and the  $S = 1/2$  EPR spectra. (c) 230 GHz EPR spectrum of 25 nm NDs. Only the  $S = 1/2$  EPR is visible. A fit is shown by the red dotted line. The fit gives  $g_{x,y} = 2.0029 \pm 0.0001$  and  $g_z = 2.0027 \pm 0.0001$  and  $1.0 \pm 0.1$  mT of Lorentzian/0.1  $\pm$  0.1 mT of Gaussian peak-to-peak line width. (d) X-band EPR spectrum of 25 nm NDs. For the fit, we used the  $g$  value for the  $S = 1/2$  spin obtained from the 230 GHz EPR measurement. The fit gives  $0.6 \pm 0.1$  mT of Lorentzian peak-to-peak line width.

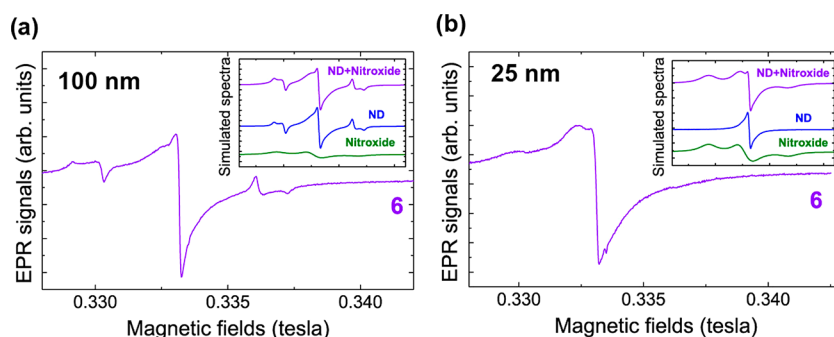


**Figure 4.** X-band cw EPR spectra of the ND powder samples (Product 6 in Scheme 1). (a) cw EPR spectrum of 100 nm NDs. The inset shows the simulated EPR spectrum consisting of ND (N plus  $S = 1/2$  impurities signal) and nitroxide EPR spectra. (b) cw EPR spectrum of 25 nm NDs. The inset shows the simulated EPR spectra consisting of ND (N only) and nitroxide EPR spectra.

functional groups to give **6**. This was confirmed by the significant reduction of the azide peak at  $2100\text{ cm}^{-1}$  in the FTIR spectra of **6**.<sup>39,40</sup> Figure 2a,b shows the FTIR peak of the azide vibrational mode at  $2100\text{ cm}^{-1}$  of Products **3** and **6**. Comparing the areas under the peaks of **3** and **6**, we estimated that approximately 95–98% of azides on the ND surface were reacted to attach nitroxide radicals. We also tested stability of the silanized surface against hydrolysis. On the basis of the FTIR intensity of the azide peak, the silanized surface is stable for more than 16 h under both water solution (pH 7.00) and slightly acidic phosphate buffer solution (pH 6.85).

Next, we employed EPR spectroscopy to confirm attachment of paramagnetic nitroxide radicals ( $S = 1/2$ ) on the surface of NDs. All EPR measurements were performed at room temperature. For X-band EPR measurements, microwave frequency of  $\sim 9.3$  GHz, applied microwave power of  $\sim 50$

$\mu\text{W}$ , and field modulation amplitude of 0.05 mT at frequency of 100 kHz were used. For 230 GHz EPR measurements, microwave frequency of 230 GHz, microwave power of  $\sim 10\ \mu\text{W}$  at sample and field modulation amplitude of  $\sim 0.05$  mT at frequency of 20 kHz were used. For measuring free nitroxide radicals aqueous solution, higher microwave power of  $\sim 5$  mW at sample was used due to attenuation of microwave power from water. Figure 3 shows 230 GHz/X-band cw EPR spectra for 100 and 25 nm NDs (Product 3 in Scheme 1). EPR spectrum in Figure 3a shows that paramagnetic impurities present in NDs consist of substitutional single nitrogen (N) impurities ( $S = 1/2$ ,  $g_{x,y} = 2.0024$ ,  $g_z = 2.0024$  and the hyperfine coupling of the N impurity to  $^{14}\text{N}$  nuclear spin ( $I = 1$ ) is  $A_x = A_y = 82$  MHz and  $A_z = 114$  MHz)<sup>4</sup> and other  $S = 1/2$  impurities.<sup>22,41</sup> By fitting the 230 GHz EPR spectrum, we extracted the  $g$  value of the  $S = 1/2$  impurities ( $g_{x,y} = 2.0029 \pm$

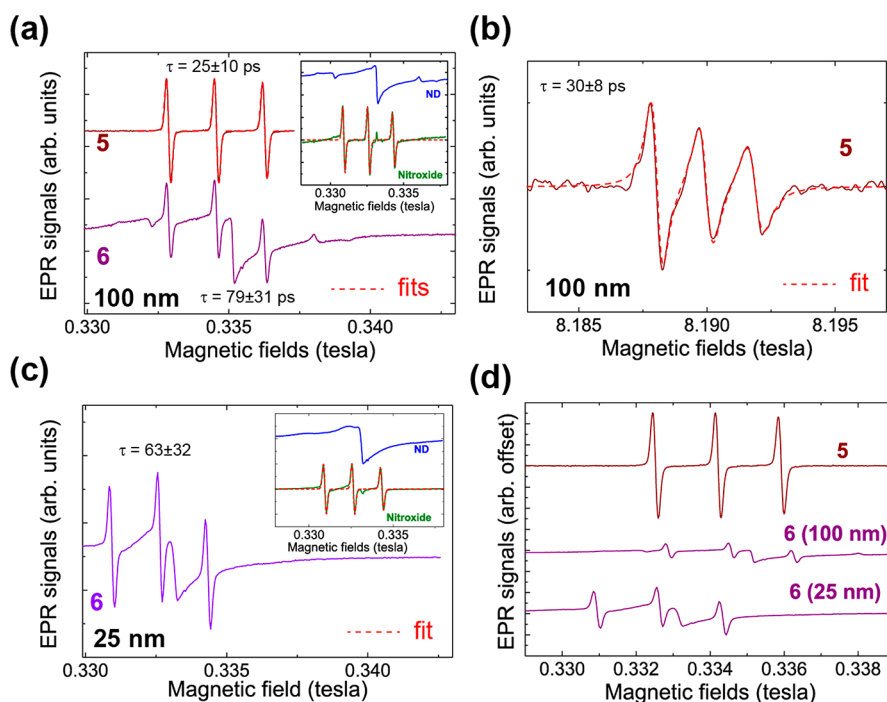


**Figure 5.** X-band and 230 GHz cw EPR spectra of 500  $\mu\text{M}$  free nitroxide radical and nitroxide radicals attached on NDs. All ND EPR spectra were measured with  $\sim 1.0$  mg of dry powder placed in a glass capillary tube, followed by the addition of 5  $\mu\text{L}$  of water. In the case of free nitroxide radicals (5), 5  $\mu\text{L}$  of 500  $\mu\text{M}$  nitroxide solution was measured. (a) X-band EPR spectra of free nitroxide radicals (5) and the nitroxide-drafted NDs (6). The fit results to extract the correlation time are shown by the red dotted line. Extracted spectrum and fit of nitroxide from the nitroxide-attached NDs are shown in the inset. (b) 230 GHz EPR spectrum of 5. Five  $\mu\text{L}$  of 500  $\mu\text{M}$  free nitroxide radical placed in a Teflon bucket. The fit result to extract the correlation time is shown by the red dotted line. (c) X-band EPR spectrum of the nitroxide-drafted NDs (6). Extracted spectrum and fit of nitroxide from the nitroxide-attached NDs are shown in the inset. The fit result to extract the correlation time is shown by the red dotted line. (d) X-band EPR spectra of 5 and 6 measured with same measurement parameters. In both samples, the same volume of 5  $\mu\text{L}$  was used. All of the volume is in the active area of the cavity; therefore, the whole sample contributes to the observed EPR signal. 6 (100 nm NDs) and 6 (25 nm NDs) include 1 mg of dry ND powders. 1:0.13:0.35 of the EPR intensity ratio (5 to 6 (100 nm NDs) to 6 (25 nm NDs)) was obtained with EPR line shape analysis.

0.0001 and  $g_z = 2.0027 \pm 0.0001$ ). To verify the  $g$  factor, we also measured the 100 nm NDs using the X-band EPR spectrometer. As seen in Figure 3b, we found a good agreement between the experimental data and the fit. In the fit, the  $g$  values for the N and  $S = 1/2$  spins were fixed to the values obtained from the 230 GHz EPR measurement and only the intensity ratio of N to  $S = 1/2$  impurities, and their linewidths were varied. In 25 nm NDs, only the  $S = 1/2$  impurities EPR signal was observed (see Figure 3c,d). This is due to lower concentration of N impurities in 25 nm NDs. From the fit,  $g_{x,y} = 2.0029 \pm 0.0001$  and  $g_z = 2.0027 \pm 0.0001$  for the  $S = 1/2$  spins were obtained, which is consistent with 100 nm NDs measurement. We also verified the  $g$  factor by comparing the X-band EPR spectrum (Figure 3d).

After characterizing Product 3 in Scheme 1, we studied cw EPR spectra of 100 and 25 nm NDs of Product 6. As shown in Figure 4a,b, the observed EPR spectra are clearly different from those of 3 because of the existence of nitroxide radicals grafted on the ND surface. To verify the results, we simulated EPR spectrum consisting of ND and nitroxides EPR spectrum. As shown in the inset of Figure 4a,b, the simulated EPR spectra agree reasonably well with the experimental results.

To confirm covalent attachment of nitroxide molecules on a ND surface, we investigated dynamics of nitroxide radicals in aqueous solution using cw EPR measurements. The spectra of 5 in Figure 5a show the X-band EPR spectrum of free nitroxide radicals in aqueous solution. Because of the motional-narrowing effect of nitroxide EPR signals, the nitroxide spectrum has three

pronounced peaks due to the hyperfine coupling of the nitroxide to  $^{14}\text{N}$  nuclear spin ( $I = 1$ ,  $A_{\text{iso}} = (A_x + A_y + A_z)/3 = 48$  MHz). Lineshape analysis of the EPR spectrum, that is, analyzing line width and amplitude of the EPR spectrum, gives the rotational correlation time  $\tau$  which indicates the degree of motion of nitroxides in aqueous solution. With the line shape analysis of the X-band EPR spectrum of 5 using easyspin,<sup>42</sup> we obtained  $\tau = 25 \pm 10$  ps. The correlation time was also estimated for 230 GHz EPR spectrum of 5. Because of the higher Larmor frequency, 230 GHz EPR measurement is more sensitive to the correlation time in the tens of picoseconds range. A fit to the 230 GHz spectrum in Figure 5b shows that the correlation time is  $\tau = 30 \pm 8$  ps, consistent with the X-band measurement. We next studied the nitroxide grafted NDs (6). Because the EPR spectrum includes both NDs and nitroxide radical signals, we first analyzed nitroxide EPR spectrum of 6 by subtracting the ND spectrum (3) with constant baseline correction (see the inset of Figure 5a). A fit was then performed to obtain the correlation time. We obtained  $\tau = 79 \pm 31$  ps for the 100 nm nitroxide-attached NDs (6). Similarly, using the EPR spectrum shown in Figure 5c, we found  $\tau = 63 \pm 32$  ps for the 25 nm nitroxide-attached NDs (6). Those slower correlation times of the nitroxide-attached on the 100 and 25 nm NDs are due to confinement of nitroxide motions; therefore, the result strongly supports successful covalent attachment of nitroxide radicals on the ND surface.

Finally, we estimated the number of nitroxide molecules grafted on the ND surface by comparing X-band EPR spectra of 5 and 6. As shown in Figure 5d, the intensity of 6 (100 nm NDs) is 13% of the 500  $\mu\text{M}$  free nitroxide radicals (5); therefore, the concentration of nitroxide radicals in 6 is  $\sim 67 \mu\text{M}$ . Given that the sample volume is  $\sim 5 \mu\text{L}$ , the number of nitroxide molecules in the sample is  $\sim 2 \times 10^{14}$ . The sample also contains 1 mg of 100 nm NDs. Using  $3.1 \text{ g/cm}^3$  for the density of 100 nm NDs<sup>43</sup> and  $\sim 5 \times 10^{-16} \text{ cm}^3$  for the volume of one 100 nm diameter spherical ND, the number on ND particles in the sample holder is  $\sim 6 \times 10^{11}$ . Thus, each 100 nm ND has  $\sim 300$  nitroxide radicals on the surface. Similarly, with  $3.52 \text{ g/cm}^3$  for the density of 25 nm NDs<sup>44</sup> and  $\sim 8 \times 10^{-18} \text{ cm}^3$  for the volume of one 100 nm diameter spherical ND, we found that each 25 nm ND has  $\sim 20$  nitroxides on the surface.

## CONCLUSIONS

We demonstrated grafting of nitroxide radicals on the ND surface using click chemistry. The reaction of the grafting was verified by FTIR spectroscopy. We also employed X-band and 230 GHz EPR spectroscopy to verify the covalent attachment of nitroxides. The EPR measurements revealed that dynamics of nitroxide molecules on a ND surface are more constrained than those of free nitroxide radicals. The observation strongly suggests successful grafting of nitroxides on NDs. We also estimated that the number of nitroxide radicals attached on a surface of NDs using the EPR method is  $\sim 300$  for 100 nm and  $\sim 20$  for 25 nm NDs.

## AUTHOR INFORMATION

### Corresponding Author

\*E-mail [susumu.takahashi@usc.edu](mailto:susumu.takahashi@usc.edu).

### Notes

The authors declare no competing financial interest.

## ACKNOWLEDGMENTS

We thank X. Zhang for support to perform the X-band EPR measurements. This work was supported by the Searle scholars program (S.T.).

## REFERENCES

- (1) Hanson, R.; Dobrovitski, V. V.; Feiguin, A. E.; Gywat, O.; Awschalom, D. D. Coherent Dynamics of a Single Spin Interacting with an Adjustable Spin Bath. *Science* **2008**, *320*, 352–355.
- (2) Childress, L.; Dutt, M. V. G.; Taylor, J. M.; Zibrov, A. S.; Jelezko, F.; Wrachtrup, J.; Hemmer, P. R.; Lukin, M. D. Coherent Dynamics of Coupled Electron and Nuclear Spin Qubits in Diamond. *Science* **2006**, *314*, 281–285.
- (3) Gaebel, T.; Domhan, M.; Popa, I.; Wittmann, C.; Neumann, P.; Jelezko, F.; Rabeau, J. R.; Stavrias, N.; Greentree, A. D.; Prawer, S.; et al. Room-Temperature Coherent Coupling of Single Spins in Diamond. *Nat. Phys.* **2006**, *2*, 408–413.
- (4) Takahashi, S.; Hanson, R.; Tol, J. v.; Sherwin, M. S.; Awschalom, D. D. Quenching Spin Decoherence in Diamond through Spin Bath Polarization. *Phys. Rev. Lett.* **2008**, *101*, 047601.
- (5) Maze, J. R.; Stanwix, P. L.; Hodges, J. S.; Hong, S.; Taylor, J. M.; Cappellaro, P.; Jiang, L.; Dutt, M. V. G.; Togan, E.; Zibrov, A. S.; et al. Nanoscale Magnetic Sensing with an Individual Electronic Spin in Diamond. *Nature* **2008**, *455*, 644–647.
- (6) Balasubramanian, G.; Chan, I. Y.; Kolesov, R.; Al-Hmoud, M.; Tisler, J.; Shin, C.; Kim, C.; Wojcik, A.; Hemmer, P. R.; Krueger, A.; et al. Nanoscale Imaging Magnetometry with Diamond Spins under Ambient Conditions. *Nature* **2008**, *455*, 648.

(7) Degen, C. L. Scanning Magnetic Field Microscope with a Diamond Single-Spin Sensor. *Appl. Phys. Lett.* **2008**, *92*, 243111.

(8) Taylor, J. M.; Cappellaro, P.; Childress, L.; Jiang, L.; Budker, D.; Hemmer, P. R.; Yacoby, A.; Walsworth, R.; Lukin, M. D. High-Sensitivity Diamond Magnetometer with Nanoscale Resolution. *Nat. Phys.* **2008**, *4*, 810–816.

(9) Holt, K. B. Diamond at the Nanoscale: Applications of Diamond Nanoparticles from Cellular Biomarkers to Quantum Computing. *Philos. Trans. R. Soc., A* **2007**, *365*, 2845–2861.

(10) Tisler, J.; Balasubramanian, G.; Naydenov, B.; Kolesov, R.; Grotz, B.; Reuter, R.; Boudou, J.-P.; Curmi, P. A.; Sennour, M.; Thorel, A.; et al. Fluorescence and Spin Properties of Defects in Single Digit Nanodiamonds. *ACS Nano* **2009**, *3*, 1959–1965.

(11) Hall, L. T.; Hill, C. D.; Cole, J. H.; Städler, B.; Caruso, F.; Mulvaney, P.; Wrachtrup, J.; Hollenberg, L. C. L. Monitoring Ion-Channel Function in Real Time through Quantum Decoherence. *Proc. Natl. Acad. Sci.* **2010**, *107*, 18777–18782.

(12) McGuinness, L. P.; Yan, Y.; Stacey, A.; Simpson, D. A.; Hall, L. T.; Maclaurin, D.; Prawer, S.; Mulvaney, P.; Wrachtrup, J.; Caruso, F.; et al. Quantum Measurement and Orientation Tracking of Fluorescent Nanodiamonds inside Living Cells. *Nat. Nanotechnol.* **2011**, *6*, 358–363.

(13) Huang, T.; Tzeng, Y.; Liu, Y. K.; Chen, Y. C.; Walker, K. R.; Guntupalli, R.; Liu, C. Immobilization of Antibodies and Bacterial Binding on Nanodiamond and Carbon Nanotubes for Biosensor Applications. *Diamond Relat. Mater.* **2004**, *13*, 1098–1102.

(14) Kong, X.; Huang, L. C. L.; Liau, S.-C. V.; Han, C.-C.; Chang, H.-C. Polylysine-Coated Diamond Nanocrystals for MALDI-ToF Mass Analysis of DNA Oligonucleotides. *Anal. Chem.* **2005**, *77*, 4273–4277.

(15) Bondar, V. S.; Pozdnyakova, I. O.; Puzyr, A. P. Applications of Nanodiamonds for Separation and Purification of Proteins. *Phys. Solid State* **2004**, *46*, 758–760.

(16) Fu, C.-C.; Lee, H.-Y.; Chen, K.; Lim, T.-S.; Wu, H.-Y.; Lin, P.-K.; Wei, P.-K.; Tsao, P.-H.; Chang, H.-C.; Fann, W. Characterization and Application of Single Fluorescent Nanodiamonds as Cellular Biomarkers. *Proc. Natl. Acad. Sci. U.S.A.* **2007**, *104*, 727–732.

(17) Neugart, F.; Zappe, A.; Jelezko, F.; Tietz, C.; Boudou, J. P.; Krueger, A.; Wrachtrup, J. Dynamics of Diamond Nanoparticles in Solution and Cells. *Nano Lett.* **2007**, *7*, 3588–3591.

(18) Huang, H.; Pierstorff, E.; Osawa, E.; Ho, D. Protein-Mediated Assembly of Nanodiamond Hydrogels into a Biocompatible and Biofunctional Multilayer Nanofilm. *ACS Nano* **2008**, *2*, 203–212.

(19) Mochalin, V. N.; Shenderova, O.; Ho, D.; Gogotsi, Y. The Properties and Applications of Nanodiamonds. *Nat. Nanotechnol.* **2011**, *7*, 11–23.

(20) Krueger, A. Beyond the Shine: Recent Progress in Applications of Nanodiamond. *J. Mater. Chem.* **2011**, *21*, 12571.

(21) Williams, O. A. Nanocrystalline Diamond. *Diamond Relat. Mater.* **2011**, *20*, 621–640.

(22) Ando, T.; Inoue, S.; Ishii, M.; Kamo, M.; Sato, Y. Fourier-Transform Infrared Photoacoustic Studies of Hydrogenated Diamond Surfaces. *J. Chem. Soc. Faraday Trans.* **1993**, *89*, 749–751.

(23) Krueger, A.; Liang, Y. J.; Jarre, G.; Stegk, J. Surface Functionalisation of Detonation Diamond Suitable for Biological Applications. *J. Mater. Chem.* **2006**, *16*, 2322–2328.

(24) Liu, Y.; Gu, Z. N.; Margrave, J. L.; Khabashesku, V. N. Functionalization of Nanoscale Diamond Powder: Fluoro-, Alkyl-, Amino-, and Amino Acid-Nanodiamond Derivatives. *Chem. Mater.* **2004**, *16*, 3924–3930.

(25) Spitsyn, B. V.; Denisov, S. A.; Skorik, N. A.; Chopurova, A. G.; Parkaeva, S. A.; Belyakova, L. D.; Larionov, O. G. The Physical-Chemical Study of Detonation Nanodiamond Application in Adsorption and Chromatography. *Diamond Relat. Mater.* **2010**, *19*, 123–127.

(26) Ida, S.; Tsubota, T.; Hirabayashi, O.; Nagata, M.; Matsumoto, Y.; Fujishima, A. Chemical Reaction of Hydrogenated Diamond Surface with Peroxide Radical Initiators. *Diamond Relat. Mater.* **2003**, *12*, 601–605.

- (27) Stober, W.; Fink, A.; Bohn, E. Controlled Growth of Monodisperse Silica Spheres in Micron Size Range. *J. Colloid Interface Sci.* **1968**, *26*, 62–69.
- (28) Liz-Marzan, L. M.; Giersig, M.; Mulvaney, P. Synthesis of Nanosized Gold-Silica Core-Shell Particles. *Langmuir* **1996**, *12*, 4329–4335.
- (29) Graf, C.; Vossen, D. L. J.; Imhof, A.; van Blaaderen, A. A General Method to Coat Colloidal Particles with Silica. *Langmuir* **2003**, *19*, 6693–6700.
- (30) Correa-Duarte, M. A.; Giersig, M.; Liz-Marzan, L. M. Stabilization of Cds Semiconductor Nanoparticles against Photodegradation by a Silica Coating Procedure. *Chem. Phys. Lett.* **1998**, *286*, 497–501.
- (31) Bruchez, M.; Moronne, M.; Gin, P.; Weiss, S.; Alivisatos, A. P. Semiconductor Nanocrystals as Fluorescent Biological Labels. *Science* **1998**, *281*, 2013–2016.
- (32) Gerion, D.; Pinaud, F.; Williams, S. C.; Parak, W. J.; Zanchet, D.; Weiss, S.; Alivisatos, A. P. Synthesis and Properties of Biocompatible Water-Soluble Silica-Coated Cdse/Zns Semiconductor Quantum Dots. *J. Phys. Chem. B* **2001**, *105*, 8861–8871.
- (33) Kolb, H. C.; Finn, M. G.; Sharpless, K. B. Click Chemistry: Diverse Chemical Function from a Few Good Reactions. *Angew. Chem., Int. Ed.* **2001**, *40*, 2004–2012.
- (34) Li, N. W.; Binder, W. H. Click-Chemistry for Nanoparticle-Modification. *J. Mater. Chem.* **2011**, *21*, 16717–16734.
- (35) Fleming, D. A.; Thode, C. J.; Williams, M. E. Triazole Cycloaddition as a General Route for Functionalization of Au Nanoparticles. *Chem. Mater.* **2006**, *18*, 2327–2334.
- (36) Binder, W. H.; Petraru, L.; Sachsenhafer, R.; Zirbs, R. Synthesis of Surface-Modified Nanoparticles Via Cycloaddition-Reactions. *Monatsh. Chem.* **2006**, *137*, 835–841.
- (37) White, M. A.; Johnson, J. A.; Koberstein, J. T.; Turro, N. J. Toward the Syntheses of Universal Ligands for Metal Oxide Surfaces: Controlling Surface Functionality through Click Chemistry. *J. Am. Chem. Soc.* **2006**, *128*, 11356–11357.
- (38) Ranjan, R.; Brittain, W. J. Tandem Raft Polymerization and Click Chemistry: An Efficient Approach to Surface Modification. *Macromol. Rapid Commun.* **2007**, *28*, 2084–2089.
- (39) Barras, A.; Szunerits, S.; Marcon, L.; Monfilliet-Dupont, N.; Boukherroub, R. Functionalization of Diamond Nanoparticles Using “Click” Chemistry. *Langmuir*, *26*, 13168–13172.
- (40) Meinhardt, T.; Lang, D.; Dill, H.; Krueger, A. Pushing the Functionality of Diamond Nanoparticles to New Horizons: Orthogonally Functionalized Nanodiamond Using Click Chemistry. *Adv. Funct. Mater.* **2011**, *21*, 494–500.
- (41) Smith, G. M.; Lesurf, J. C. G.; Mitchell, R. H.; Riedi, P. C. Quasi-Optical Cw Mm-Wave Electron Spin Resonance Spectrometer. *Rev. Sci. Instrum.* **1999**, *69*, 3924.
- (42) Stoll, S.; Schweiger, A. Easyspin, a Comprehensive Software Package for Spectral Simulation and Analysis in Epr. *J. Magn. Reson.* **2006**, *178*, 42.
- (43) Engis Corporation. <http://www.engis.com/> (accessed April 16, 2011).
- (44) Van Moppes Corporation. <http://www.vanmoppes.ch/> (accessed August 15, 2011).